



Article

Ice Hydrometeor Shape Estimations Using Polarimetric Operational and Research Radar Measurements

Sergey Y. Matrosov

Cooperative Institute for Research in Environmental Sciences, University of Colorado and NOAA Earth System Research Laboratory, Boulder, CO 80309, USA; Sergey.Matrosov@noaa.gov

Received: 26 December 2019; Accepted: 10 January 2020; Published: 14 January 2020



Abstract: A polarimetric radar method to estimate mean shapes of ice hydrometeors was applied to several snowfall and ice cloud events observed by operational and research weather radars. The hydrometeor shape information is described in terms of their aspect ratios, r, which represent the ratio of particle minor and major dimensions. The method is based on the relations between depolarization ratio (DR) estimates and aspect ratios. DR values, which are a proxy for circular depolarization ratio, were reconstructed from radar variables of reflectivity factor, Z_e , differential reflectivity, Z_{DR} , and copolar correlation coefficient ρ_{hv} , which are available from radar systems operating in either simultaneous or alternate transmutation of horizontally and vertically polarized signals. DR-r relations were developed for retrieving aspect ratios and their sensitivity to different assumptions and model uncertainties were discussed. To account for changing particle bulk density, which is a major contributor to the retrieval uncertainty, an approach is suggested to tune the DR-r relations using reflectivity-based estimates of characteristic hydrometeor size. The analyzed events include moderate snowfall observed by an operational S-band weather radar and a precipitating ice cloud observed by a scanning K_a -band cloud radar at an Arctic location. Uncertainties of the retrievals are discussed.

Keywords: polarimetric radar; depolarization ratio; snowfall; ice clouds; hydrometeor shape

1. Introduction

Scanning polarimetric weather radars operating at centimeter-wavelength frequency bands, such as S (~3 GHz), C (~5 GHz) and X (~10 GHz) bands, have been long used for hydrometeor identification (HID) retrievals [1–3]. The HID algorithms usually utilize a fuzzy-logic approach and are based on variables from horizontal and vertical polarization radar measurements such as the equivalent radar reflectivity factor (hereafter just reflectivity), Z_e , differential reflectivity, Z_{DR} , specific differential phase K_{DP} , and copolar correlation coefficient, ρ_{hv} . As an output, these algorithms prescribe different dominant hydrometeor types/species for cloud and precipitation particles filling the radar resolution volume. Typical ice hydrometeor species that are routinely identified using radar measurements are hail, graupel, aggregated snow, and ice crystals. Quantitative information on ice particle shapes, however, is not typically provided by the HID algorithms.

Atmospheric ice particles, however, have a great variety of habits and most commonly, they are of irregular shape [4]. In many practical applications ranging from microphysical and climate modeling studies [5,6] to snowfall quantitative precipitation estimation (QPE) methods [7], a general shape type of ice hydrometeors needs to be quantified. Usually, simple oblate spheroidal shape (for planar type crystals) or prolate spheroidal shape (for columnar type crystals) models are used for describing irregular ice particle shapes [8]. An aspect ratio defined as the ratio of particle minor

and major dimensions is a general parameter-characterizing particle shape. While the spheroidal shape has limitations in describing the hexagonal structure of single pristine ice crystals, it is generally appropriate for describing a degree of non-sphericity of irregular shape particles which often are a dominant species.

A remote sensing method for estimating mean aspect ratios for relatively homogeneous horizontal layers of precipitating ice hydrometeors using direct measurements of circular depolarization or slant 45° linear depolarization ratios (CDR and SLDR, respectively) was suggested and applied to data taken by scanning millimeter-wavelength frequency (~35 and ~95 GHz) cloud radars [9,10]. CDR and SLDR measurements unlike a traditional horizontal—Vertical polarization linear depolarization ratio (LDR)—are not very sensitive to particle wobbling around preferential orientation with major dimensions in the horizontal plane, so these measurements are suitable for inferring particle shapes. Standard deviations of particle wobbling are usually smaller than about 30° [11,12]. A similar remote sensing method was also later applied for fully polarimetric K_a -band scanning radar measurements [13]. While this radar did not directly measure CDR, CDR values were reconstructed from linear polarization basis measurements as in [14]. Radar-based retrievals of particle aspect ratios in these studies agreed generally well with concurrent in-situ measurements when appropriate particle density assumptions were made

Recently [15,16], suggested an approach to reconstruct depolarization ratio (DR) from Z_{DR} and ρ_{hv} observations by radars operating in the simultaneous transmission-simultaneous reception (STSR) mode, which precludes direct measurements of depolarization. Later, weather radar Z_{DR} and ρ_{hv} measurements were applied to infer aspect ratios of ice cloud hydrometeors assuming the solid ice hexagonal particles, which are characteristic of single plates or solid columns [12]. Moreover, depending on particle shapes, observed polarimetric variables also depend on particle bulk density, so density assumptions are essential for aspect ratio retrievals from depolarization [9] or combined Z_{DR} and ρ_{hv} measurements [17]. For the soft spheroidal particle model, the particle bulk density assumption is, in essence, equivalent to an assumption of the complex dielectric constant of the ice-air mixture which dry hydrometeors are made of. Without the density assumption, only a polarizability parameter of the particles can be estimated [17]. The objective of this study was to extend depolarization-based ice hydrometeor shape retrievals to evaluate the spatial variability of their aspect ratios with approximate accounting for the effects of changing particle density.

2. Models and Methods

A logarithmic scale proxy of depolarization ratio (DR) obtainable from STSR horizontal (*h*) and vertical (*v*) polarization measurements can be expressed as [15,16]

$$DR(dB) = 10 \log_{10} \left[(Z_{dr} + 1 - 2 Z_{dr}^{0.5} \rho_{hv}) / (Z_{dr} + 1 + 2 Z_{dr}^{0.5} \rho_{hv}) \right]$$
(1)

where Z_{dr} is differential reflectivity in the linear scale (i.e., logarithmic scale $Z_{DR} = 10 \log_{10}(Z_{dr})$. For STSR measurements, DR depends on the transmitter phase shift between h and v polarized signals (ϕ_t), which often is not known. It has been shown [16] that this dependence is usually rather weak. While being only a proxy for othe ircular depolarization ratio, the DR parameter has important advantages over real depolarization measurements. It does not depend on propagation phase shift as true CDR [18]. DR estimates are available in all radar resolution volumes where directly measured co-polarized signals are reliably measured. The real depolarization measurements, on the other hand, are only available when weak depolarized echoes are reliably measured, which greatly diminishes radar coverage for depolarization ratios compared to reflectivity [10]. DR estimates, in essence, combine the information contained in Z_{DR} and ρ_{hv} for more convenient retrievals of particle aspect ratios.

Modeling the mean particle aspect ratio—DR correspondences—is performed in this study assuming oblate spheroidal particles in the Rayleigh scattering regime which is generally valid for atmospheric ice hydrometeors at S-band frequencies. An oblate general habit for snowflakes was

used in many previous modeling studies [4,9,16,19]. The oblate vs. prolate general habit identification used in many previous modeling studies [4,9,16,19]. The oblate vs. prolate general habit identification is possible using trends of radar elevation angle dependencies of DR [8,9]. Observations, however, is possible using trends of radar elevation angle dependencies of DR [8,9]. Observations, however, indicate that compared to oblate planar-type habit, prolate (e.g., columnar) particle types (while not uncommon) are rarely a dominant habit of precipitating ice [2,0,21]. Details of calculating Z_{dr} and ρ_{lv} for spheroidal ice particles in the STSR measurement mode are Details of calculating Z_{dr} and ρ_{lv} for spheroidal ice particles in the STSR measurement mode are given in [15,16]. To model aspect ratio (r)-DR relations for particle populations, it was assumed that the particle size distribution (PSD), as a function of particle major dimension, D, is described by the gamma-function: $N(D) = N_{\theta} \exp[-(3.67 + \mu)D/D_{rtv}], \qquad (2)$

$$N(D) = N_0 \exp[-(3.67 + \mu)D/D_{mv}]$$

$$N(D) = N_0 \exp[-(3.67 + \mu)D/D_{mv}]$$
(2)

where N_{θ} , μ are the intercept and width parameters (note that DR is immune to changes in N_{θ}), and D_{mv} where N_{θ} , μ are the intercept and width parameters (note that DR is immune to changes in N_{θ}), and D_{mv} is the median volume particle size, which represents the characteristic PSD size. Due to aerodynamic is the median volume particle size, which represents the characteristic PSD size. Due to aerodynamic forcing, falling particles tend to be oriented with their major dimensions in the horizontal plane, forcing, falling particles tend to be oriented with their major dimensions in the horizontal plane, so it was assumed that the mean canting angle θ is zero. Particle wobbling around the preferential horizontal orientation was described by the Gaussian distribution with respect to θ with the standard deviation σ_{θ} .

deviation σ_0 .

deviation σ_0 .

The mass of individual particles, m, was modelled in a customary way using a power-law The mass of individual particles, m, was modelled in a customary way using a power-law approximation: $m = aD^b$.

(3)

where a and b are empirical coefficients. The corresponding bulk density was calculated by dividing where a and b are empirical coefficients. The corresponding bulk density was calculated by dividing particle mass by the spheroidal volume and it was capped by the solid ice density maximum value of particle mass by the spheroidal volume and it was capped by the solid ice density maximum value of 0.916 g cm⁻³. A minimum value of 0.010 g cm⁻³ was assumed when the use of m-D relations for larger 0.916 g cm⁻³. A minimum value of 0.010 g cm⁻³ was assumed when the use of m-D relations for larger particles resulted in values less than 0.01 g cm⁻³. Depending on the bulk density, the particle dielectric particles resulted in values less than 0.01 g cm⁻³. Depending on the bulk density, the particle dielectric constant was calculated using the Maxwell–Garnet mixing rule for air-solid ice mixtures. Constant was calculated using the Maxwell–Garnet mixing rule for air-solid ice mixtures. Figure 1 shows the results of modeling particle r-DN relations for the radar elevation angle $\alpha = 10^{\circ}$, transmitter phase shift $\phi_1 = 90^{\circ}$ (i.e., circular polarization is transmitted), the exponential particle size distribution (i.e., $\mu = 0$) and moderate particle woobling ($\sigma_0 = 20^{\circ}$). The antenna polarization isolation, which is characterized by the minimal value of measurable LDR, was assumed to be -27 dB. This value is typical for many research and operational radars, including the ones used in previous studies [13]. The coefficients in the m-D relation were assumed to be a = 0.0053 and a = 2.1 (m is in grams, D is in cm). These coefficients were found to be suitable for low-to-moderately rimed snowlakes [21]. The coefficients were found to be suitable for low-to-moderately rimed snowlakes [22]. They also practically coincide with coefficients found independently [23] based on a large dataset of in situ measurements. DR for particles with r < 0.1 were not modeled. Such low aspec

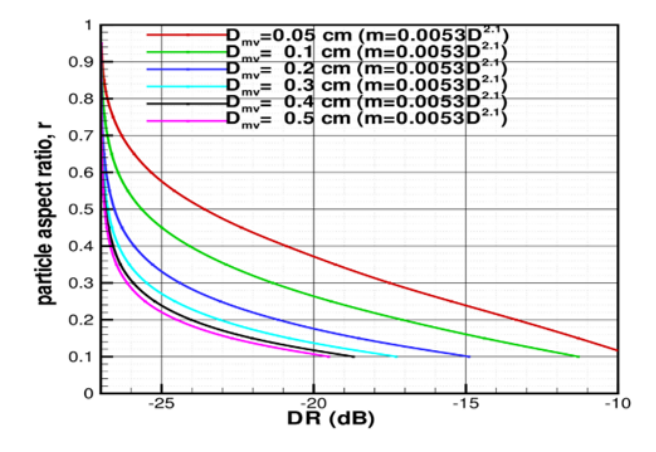


Figure 1. r-IDR relations for different values of median volume particle size, D_{mv} , assuming that the radar elevation angle $\alpha = 10^{\circ}$, transmission phase shift $\phi_{t} = 90^{\circ}$, the standard deviation of particle woldsling $\sigma_0 = 20^\circ$, and $m = 0.0053D^{2.1}$ mass-size relation (m is in grams, D is in cm).

Atmosphere **2020**, 11, 97 4 of 14

As seen from Figure 1, there is a strong variability in the r-DR relations due to changes in D_{mv} . Since free by drameters scattering at S-band is generally in the Rayleigh regime, this variability is 4 due to changing particle density, as it is proportional (for a given value of particle aspect ratio) to D^{b-3} . Dense rparticles of the same shape cause stronger dispolarization of observed radiance hoes. For given particle shapes, ISD type and the m-Drebtion, D_{mv} can be considered as a proxy for an ensemble averaged particle density, so it can be possible to account for the density effect on DR through the changes in D_{mv} . Independent information on particle characteristic size, however, from the sources other than adatament are geig, situ sticrophysically observations) ally usually ilables another, for aparticle aparticle administrational sensors.

Retentially dialaterage recyclatic (RBR) declare an usementer as provide infermation at θ_{n} and θ_{n} . The isotherse constructed mass measurements between a social drawing the construction of the principal con

$$D_{mv}^{D_{mv}} = 0.095 Z_{\rho}^{0.94} \tag{4}$$

where D_{mv} is in cm and Z_e is in mm 6 m 3 . As found from modeling using in-situ PSDs, the data scatter where D_{mv} is in cm and Z_e is in mm 6 m 3 . As found from modeling using in-situ PSDs, the data scatter where D_{mv} is in the property of the pr

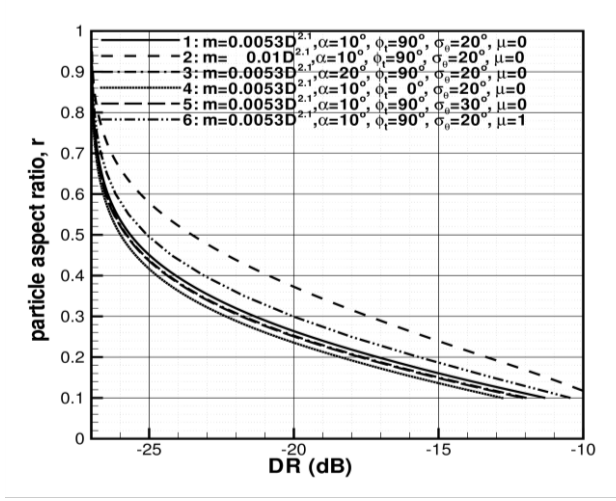


Figure 2. *r*-DR relations assuming $D_{mv} = 0.1$ cm and different assumptions for the radar elevation angle **Figure 2.** *r*-DR relations assuming $D_{mv} = 0.1$ cm and different assumptions for the radar elevation angle α, transmission phase shift φ_t , the standard deviation of particle wobbling σ_θ , and the coefficients in the particle mass-size relation.

As seen from Figure 2, changes in the horizontal-vertical polarization phase shift on transmission typically cause a rather modest variability in the r-DR relations. For a given DR values, changes in ϕ_t (curve 4 vs. curve 1 in Figure 2) from 90° (i.e., circular polarized signals are transmitted) to 0° (i.e., 45° slant linearly polarized signals are transmitted) result in the variability of particle aspect ratios of an order of only few hundredths. This is, in part, due to the fact that DR remains a good proxy for CDR corrected for propagation phase shift even though ϕ_t can change rather significantly

Atmosphere 2020, 11, 97 5 of 14

(curve 4 vs. curve 1 in Figure 2) from 90° (i.e., circular polarized signals are transmitted) to 0° (i.e., 45° slant linearly polarized signals are transmitted) result in the variability of particle aspect ratios of an Atmosphere 2020-11, x FOR PEER REVIEW order of only few hundredths. This is, in part, due to the fact that DR remains a good proxy for CDR opereded for propagation plans is hist even though angean change at the visionificantly (1 floor similarly) small variability is coused by changes in the radarisles ation angle and the radarisles at the radaris in Figure 2) ce Note that 130% is the large styles asign) and erused with the Weather Surveillance Radar 1988 Pransleris WSR-p882) sperational investorier dan network e Ladike the transmission phase shift us known, is other rubkneys; the radar elevation and leafur each scan is known, so the r-DR relations can be easily adjusted for each to the radar configuration parameters, changes in particle microphysical property assulfondared to the tradern soon figure tide rearranging in hange Dir particles microphysical propertyassummations could sourcompre optic; able exprincility in the 6-PR relation the 4-change tiouther and cit some of unctional of the first of the state Changes along therrerials have particularly fixed by the particular and the particular description of the particular descripti chapses in the softicisets in the particle mass-vize relation ranselastor which causes there chapses is nesticle rimins creates the rimins is no saverethat a grownele tage is peached in mins processes erasults inagetin cross and the coefficient gip Equation (3) radials the exponent hin this equation remains mostly unchanger 12the Charges awabout a factor of 2 in a which corresponds to rather 1 strong rizying, shift the r-DRerelation by droute 1-10 to neather are selective 2 remarked with the rather modest (curve 5 vs. The sensitivity of the Thirtiselations to continuous arientation by obeling is, when modesther year warfauresenintfieureparticieinispes. impententand vanteen en Prankee Wooderhichais aneether, entere variable sensitive to particle shapes when the rame value of the particle weekeling wave meter one there is a greater on a register denote have an Dreams Zean is his regression denote bevieved, chances exist of casansbown, in Figure frew here modeling creal to of this correspondence are, depicted for two notating fr assumptions which differently by called by Jon Compared to 6-Principline it have attended from the property variabilitativa tha 162 procelations caused burnecentainties in valuation point is illustrated in Figure of where both it lation transported bound on different appropriate both it lation transported by the control of th PRote particle orientations/webblingsmakestelanelarization-based asstematas of marticle, aspect ratios more robust compared to potential differential reflectivity-based aspect ratio estimates.

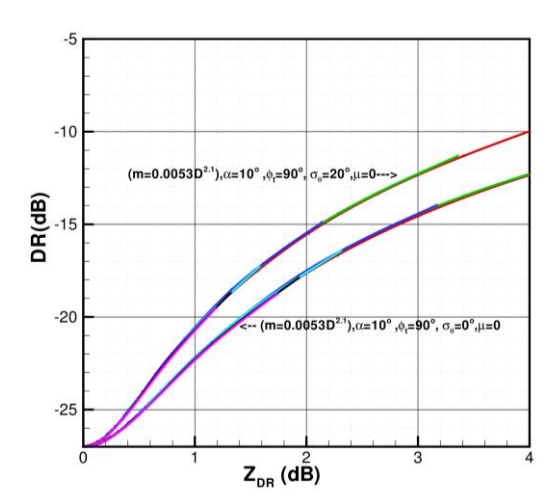


Figure 3. *r*-DR relations assuming $D_{mv} = 0.1$ cm and different assumptions for the radar elevation angle **Figure 3.** *r*-DR relations assuming $D_{mv} = 0.1$ cm and different assumptions for the radar elevation angle α, the transmission phase shift φt, the standard deviation of particle wobbling $σ_θ$, and the coefficients α, the transmission phase shift φt, the standard deviation of particle wobbling $σ_θ$, and the coefficients in particle mass-size relation. Different color segments correspond to results of modeling with different in particle mass-size relation. Different color segments correspond to results of modeling with D_{mv} values (i.e., 0.05, 0.1, 0.2, 0.3 and 0.5 cm).

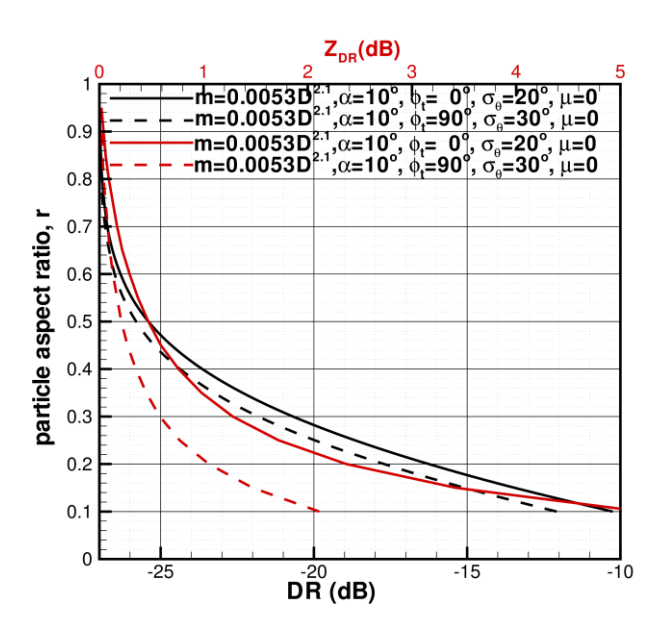


Figure 4. *r*-DR (lower *X*-axis, black curves) and r- Z_{DR} (upper *X*-axis, red curves) relations for different Figure 4. *r*-DR (lower *X*-axis, black curves) and r- Z_{DR} (upper *X*-axis, red curves) relations for different particle wobbling parameters σ_{θ} .

Different sources of retrieval errors discussed above can be considered independent. Accounting for positificent sources of retrieval errors discussed above sources of maintended and considered independent. Accounting for positificent sources of retrieval errors discussed above sources of maintended and considered independent of the position of the position of the position of the properties of particles of particles of the position of the properties of the p

33! Results of of the Retrievals Using Operational Weather Radars

The next generation radar (NEXRAD) network of the United States National Weather Service (NWS) consists of about 160 WSR-88DS-band units which employ the horizontal-vertical polarization STSR Theamusement mode. Ther WIRE SER ID prizon taken of a hization or Bratis in a differential traffectivities andvospolansumelationbougfficientworebsidaspandrealymovailakin fromptoe NationalicimaticeDatal Genterization et subversure meannale de TMSRVSRD et de un entre par de la company de l particle size and appealaration retains also different sported area which was exhibited from 5 that that 20 hall reanlake Superionter prizicular SNVS operationalizada vistrisso social broatechats and tito de operational 43NamabasuapaanaesilevahAMSbdaeariDulutbvAVianenga(466886ABevIn924316A8v4Vdbudveson fourtlatter 2 deporture of the control of the contr Figure 1 is 14 about 4 do not the acres is 14 27 MSC). According to the sound 4 do 18 acres of the acres is 14 27 MSC). According to the acres is 14 27 MSC). ave) manti fested by a very to welent frier Klock I. P.R. Penticle report to raing et rieval a mone performed with that assumptioned which use Bisusest to generate the modeling 1992 Its Towns is Bisussible grophthal ther actual tradatibeame levertices terretices terretices and order of the leverted specifixed that hopes improved a release and the control of the co factorecapterting hulle chansity de Boath Direlation anothicients a RSD advopolter high rearragin reactus, desire resident mortiables lensitive to the changes in the radar elevation angle in the range 0°-20° as compared to influencing factors affecting bulk density (e.g., m-D relation coefficients, a PSD shape), which is a major factor defining radar variables [27].

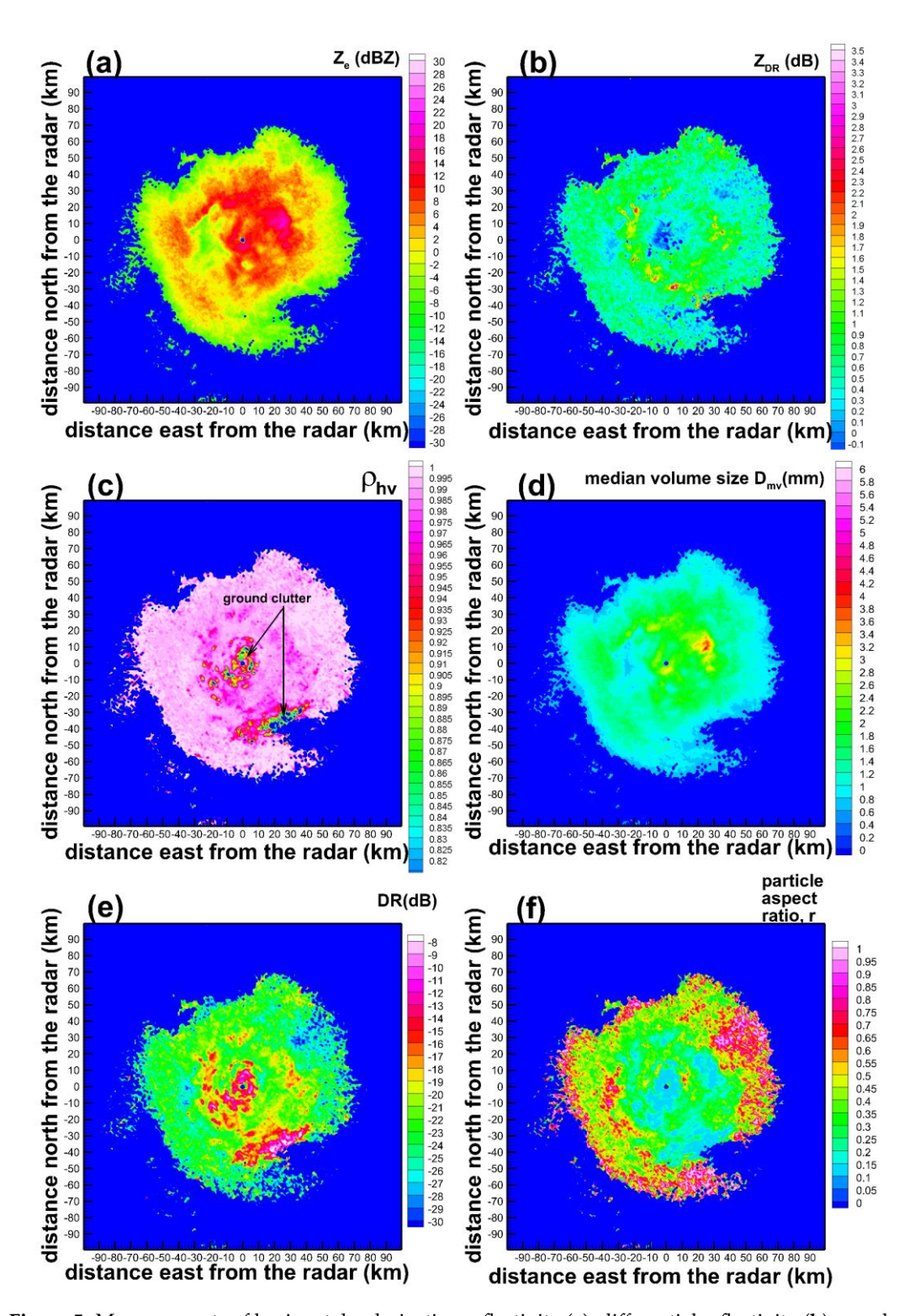


Figure 5. Measurements of horizontal polarization reflectivity (a), differential reflectivity (b), copolar regrets of Measurements of horizontal polarization reflectivity (a), differential reflectivity (b), copolar correlation coefficient (c), estimates of depolarization ratio (e) and retrievals of particle median, volume correlation coefficient (c), estimates of depolarization ratio (e) and retrievals of particle median size (d) and aspect ratio (f) corresponding to a KDLH radar scan at 4.5° on 5 March 2013 at 19:27 UTC. volume size (d) and aspect ratio (f) corresponding to a KDLH radar scan at 4.5° on 5 March 2013 at

For the scan shown in Figure 5, DR based retrievals of aspect ratios at distances closer than about 40 km generally indicate moderately non-spherical particles with pockets of particles with lower aspect For the scan shown in Figure 5, DR based retrievals of aspect ratios at distances closer than about ratio values, which approximately coincide with regions of larger ZDR values. At further radar ranges 40 km generally indicate moderately non-spherical particles with pockets of particles with lower there is a tendency for more spherical particles. These ranges correspond to higher altitudes above the aspect ratio values, which approximately coincide with regions of larger ZDR values. At further radar ground (e.g., at the 4.6° elevation the center of the radar beam is at an altitude of about 3.2 km above ranges there is a tendency for more spherical particles. These ranges correspond to higher altitudes above the ground (e.g., at the 4.6° elevation the center of the radar beam is at an altitude of about 3.2

Atmosphere **2020**, 11, 97 8 of 14

the ground for a 40 km range). An exception for this general tendency is a region at about 50 km to the south-east from the radar site, where locally higher values of Z_{DR} and lower ρ_{hv} values result in higher DR, which indicates rather non-spherical particles. Radiosonde sounding from the location in Chanhassen, MN (not shown) indicated that during radar measurements, temperatures at altitudes of about 3.2 km above ground were approximately -15 °C, which corresponds to a temperature regime favorable for the growth of dendritic crystals with low aspect ratios [28]. This might explain the transition between dominant shapes happening at radar ranges of around 40–50 km. Measurements at longer ranges, however, should be treated with some caution, as lower signal-to-noise ratios (SNRs) can cause biases in observed polarimetric variables [29]. To avoid very low SNRs, data points were considered only if reflectivities were greater than -10 dBZ.

Another example of KDLH radar measurements and corresponding particle characteristic size and aspect ratio retrievals is shown in Figure 6. The snowfall event depicted in Figure 6 was observed on 20 February 2014. It can be seen that for this event, very non-spherical particles were present in the entire area of the north-eastern quadrant (i.e., between azimuthal directions of 0° and 90°) and also at close distances in the south-west direction. High values DR and Z_{DR} and low ρ_{hv} values observed in these areas are indicative of dendritic-type pristine crystals being a dominant hydrometeor habit. According to the radiosonde soundings, the -15 °C level for this measurement time was at about 4 km above the ground (i.e., at approximately a 50 km range from the radar site). Note also that reflectivities across these areas vary very significantly, which results in a large dynamic range of particle median volume size estimates (e.g., from about 1 mm to approximately 4 mm). Almost everywhere else in the depicted scan particles are more spherical with aspect ratios of about 0.4–0.9 which are characteristic of irregular hydrometeor shapes. As for the event shown in Figure 5, the particle mean aspect ratio data in Figure 6 at further radar ranges (and thus at higher altitudes) are near 0.9–1.0 and rather noisy, which might be, in part, due to low SNR values and the influence of particle tumbling.

Potential Z_{DR} biases will cause uncertainties in DR calculations and thus influence aspect ratio retrievals. Modeling with the DR Estimator (1) indicates that for a 0.1 dB Z_{DR} bias and typical values of ρ_{hv} (e.g., $0.85 < \rho_{hv} < 0.995$), errors in DR estimates are generally less than about 0.5 dB for smaller Z_{DR} values (e.g., 0.2 dB $< Z_{DR} < 1.5$ dB). For larger Z_{DR} values, these errors generally diminish. The data in Figure 1 suggest that such DR errors can correspond to an additional uncertainty of aspect ratio retrievals of the order of several hundredths.

3.2. An Example of the Retrievals Using a Research Cloud Radar

Millimeter wavelength cloud radars operating at frequencies of around 35 GHz and 95 GHz have been also used for snowfall measurements at shorter ranges [30]. Recently, mean aspect ratios of ice hydrometeors observed at a given altitude were retrieved using K_a -band (~35 GHz) radar polarimetric measurements at the U.S. Department of Energy's (DOE) Atmospheric Radiation Measurement (ARM) Program mobile facility in Oliktok Point (70.495° N, 149.886° W), Alaska [13]. The Scanning ARM Cloud Radar (SACR) used for these retrievals transmits horizontally and vertically polarized signals alternatively, which alleviates cross-coupling effects in the differential reflectivity data, and measures horizontal-vertical polarization linear depolarization ratio (LDR) directly, thus allowing estimations of DR, which, in this case, is the proxy of true CDR without unwanted effects of the propagation phase shift [14].

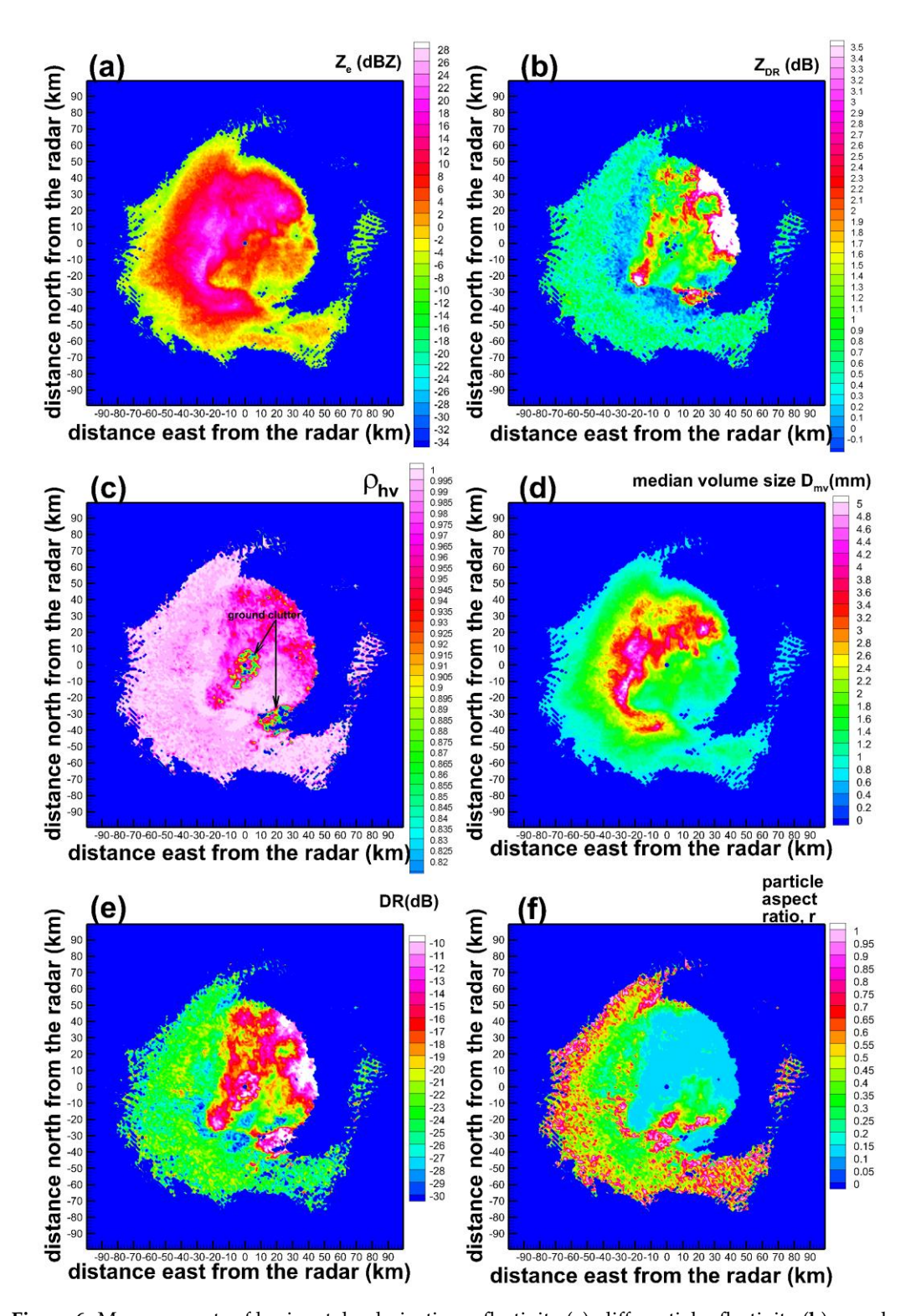


Figure 6. Measurements of horizontal polarization reflectivity (a), differential reflectivity (b), copolar Pigure 6. Measurements of horizontal polarization reflectivity (a), differential reflectivity (b), copolar correlation coefficient (c), estimates of depolarization ratio (e) and retrievals of particle median volume correlation coefficient (c), estimates of depolarization ratio (e) and retrievals of particle median size (d) and aspect ratio (f) corresponding to a KDLH radar scan at 4.5° on 20 February 2014 at volume size (d) and aspect ratio (f) corresponding to a KDLH radar scan at 4.5° on 20 February 2014 at 19:31 UTC.

The retrievals in [13] were performed for the range-height indicator (RHI) SACR measurements 3.2. An Example of the Retrievals Using a Research Cloud Radar and 40° radar elevation angle data were used for aspect ratio retrievals. This specific elevation angle was chlosidinterinival the third that were used for aspect ratio retrievals. This specific elevation angle was chlosidinterinival the third that the transfer of the transfer of the second ratio of the hydrometeors observed at a given altitude were retrieved using Ka-band (~35 GHz) radar polarimetric measurements at the U.S. Department of Energy's (DOE) Atmospheric Radiation

aspect ratios near the radar location but it is rather limited for the purpose of evaluating larger scale spatial variability of hydrometeor shapes as a function of the azimuthal direction and the distance from the radar site. The plan position indicator (PPI) azimuthal scans at low elevation angles, which are similar to those performed by the NEXRAD radars, are convenient for this purpose. In addition to the RHI scans, the SACR also regularly performs such PPI scans [31], which are used here to illustrate the aspect ratio retrievals for larger spatial regions using the same approach as that described above for applications with operational weather radars. It should be noted, however, that cloud radars typically have smaller maximum observational ranges but provide better spatial and angular measurement resolutions compared to operational WSR-88D observations.

An example of SACR PPI measurements and corresponding retrievals for a precipitating ice cloud observed on 21 October 2016 at around 00:52 UTC is shown in Figure 7. The color scales of radar variables and corresponding microphysical retrievals are the same as for the WSR-88D data shown in Figures 5 and 6, though the SACR maximum range is significantly smaller. The SACR PPI radar elevation angle for the data in Figure 7 was 5°. There is an obvious partial radar beam blockage from local structures at a relatively narrow angle intervals centered at azimuths of about 152°, 165°, and 341°. This blockage is most pronouncedly seen in reflectivity measurements (Figure 7a). There is also an arc of ground clutter which is best seen in depolarization data (Figure 7e), as DR is also a good tool for clutter identification. The estimates of particle aspect ratios and characteristic sizes for the regions of partial beam blockage and clutter should be ignored.

Estimates of the median volume particle size (Figure 7d) were performed using the Z_e - D_{mv} relation obtained specifically for the K_a-band frequencies from the large in situ microphysical dataset [26]. It was assumed that the particle size distribution for the event time shown in Figure 7 had an exponential form as it was indicated by closely collocated in time in situ measurements using Video Ice Particle Sampler (VIPS), which was launched on a tethered balloon near the radar site [13]. The VIPS instrument provides quantitative information on particle size distributions and shapes. As seen from Figure 7d, estimated D_{mv} values were generally smaller than about 1.5 mm in the larger area of observations and around 0.8–1 mm in the vicinity of the radar site. This agrees well with VIPS estimates of $D_{mv} \approx 0.08$ mm which were obtained near the radar site at a balloon altitude of about 0.5 km at around the time of radar observations shown in Figure 7.

The particle mean aspect ratios retrieved from the SACR measurements are shown in Figure 7f. The retrievals were performed based on depolarization ratio estimates using the approach discussed in Section 2. It can be seen that there was a pronounced change in aspect ratios in the region of observations. More spherical particles were present in the north-western half of the observational area while hydrometeors with larger degree of non-sphericity (i.e., smaller aspect ratios) were present in the south-western half. Aspect ratio values in the vicinity of the radar site were around 0.4–0.5, which is in good agreement with estimates of about 0.5 from in-situ VIPS measurements at around the time of observation [13]. As is the case with the most radar-based measurements, the retrievals are generally representative for the larger particles as power radar parameters (in the scattering Rayleigh regime) are approximately proportional to the fourth moment of the particle size distribution (for typical values of exponent $b \approx 2$ in Equation (3)). It should be mentioned, however, that the VIPS data indicated that there was no significant dependence of aspect ratios of individual particles on their size, as observed from in-situ measurements [13].

Maximum observed reflectivities (Figure 7a) were approximately 5 dBZ and estimated D_{mv} values were generally less than 1.5 mm. At these reflectivity levels, non-Rayleigh scattering effects at K_a -band are expected to be rather small [32]. For larger particle populations, however, these effects could be substantial and need to be accounted for in the retrievals. Especially important accounting for non-Rayleigh effects would be for the retrievals at W-band (~94 GHz) cloud radar frequencies [6]. Signal attenuation at W-band frequencies, however, is usually much more severe compared to lower frequencies [33], so sensible retrievals often could be available only for closer ranges.

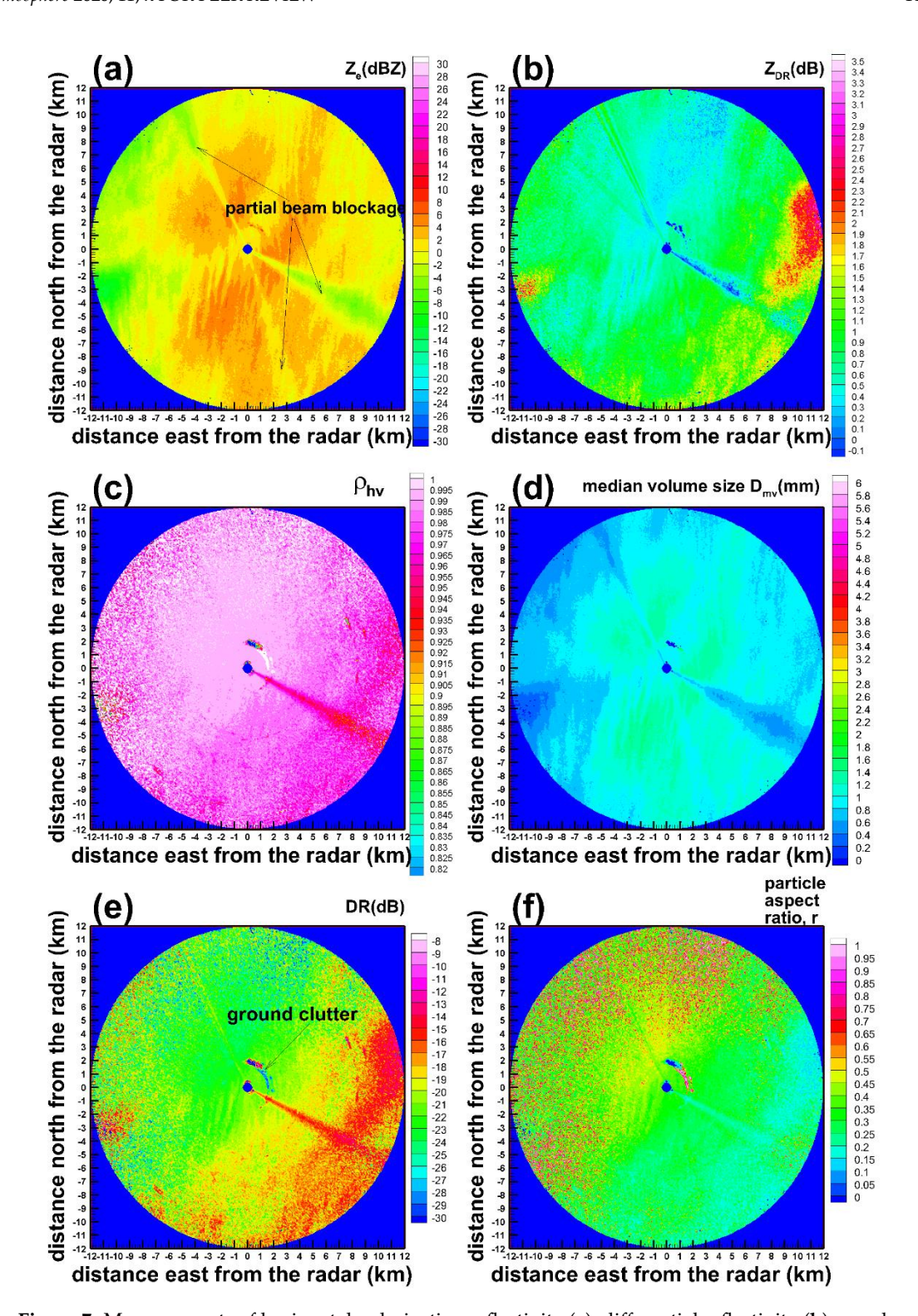


Figure 7-Massurments of Protezonal polarization reflectivity, (1), differential reflectivity, (1), coplar correlation reflection reflection reflection for the particle of particle of the particle of particle of the particl

As seen from Figure 7f (and also Figures 5f and 6f), retrievals of aspect ratios are rather noisy, even though the gradual changes in mean particle shapes over the observational domain are quite. The particle mean aspect ratios retrieved from the SACR measurements are shown in Figure 7f. identifiable. The uncertainty of the SACR-based mean aspect ratio retrievals as estimated theoretically. The retrievals were performed based on depolarization ratio estimates using the approach discussed and from comparisons with in situ observations was about 0.1–0.15 when depolarization at 40° in Section 2. It can be seen that there was a pronounced change in aspect ratios in the region of elevation was used for retrievals [13]. For the lower elevation angle observations shown in this study, observations. More spherical particles were present in the north-western half of the observational area while hydrometeors with larger degree of non-sphericity (i.e., smaller aspect ratios) were present

retrieval uncertainties could be higher as the effects of particle orientation/tumbling on DR values become stronger.

4. Conclusions

Quantitative information about general shapes of atmospheric ice particles is important for many practical applications such as the development of novel polarimetric snowfall QPE methods and advanced modeling of microphysical processes involving evolution of ice hydrometeors. Depolarization ratio (DR) estimates, which are less susceptible to particle orientations compared to other polarimetric variables such as differential reflectivity, can be readily deduced from polarimetric radar variables measured directly. These estimates are a convenient tool for estimating an average particle shape in terms of the mean aspect ratio, r, which represents the ratio of particle minor and major dimensions.

In addition to the particle shape, DR values strongly depend on particle bulk density; thus, density information is essential for meaningful aspect ratio retrievals. As in situ microphysical studies show, the mass of individual ice particles, m, is strongly related to their size, D. Knowing a characteristic hydrometeor size (e.g., median volume size, D_{mv}) representing the whole particle size distribution allows for implicit accounting for the density information in the radar-based aspect ratio retrievals. DR-r relations used in the retrievals were derived as a function of D_{mv} . The mass-size (m-D) relations, which are representative for unrimed and low-to-moderately rimed atmospheric ice particles, were used in these derivations.

Independent information on particle characteristic sizes (e.g., from other remote or direct sensors) could enhance aspect ratio retrievals. Due to the absence of such independent information in this study, the D_{mv} estimates used in the aspect ratio retrievals were obtained from the reflectivity measurements. These estimates are based on a relatively high correlation between D_{mv} and Z_e , which was demonstrated using a wide range of in situ observations in precipitating ice clouds [26].

The suggested polarimetric radar-based approach for retrievals of atmospheric ice particle aspect ratios was applied to low radar elevation angle (\sim 4.5°) azimuthal measurements from an operational WSR-88D unit located near Duluth, MN and a research scanning cloud radar deployed in Oliktok Point, AK. WSR-88D measurement examples during two different moderate snowfall events indicated a general change in particle habits from rather spherical hydrometeors with aspect ratios of around 0.6 and larger to more non-spherical particles with aspect ratios less than about 0.4 at radar ranges that approximately corresponded to the altitudes of the -15 °C isotherm, which is the temperature favorable to the dendritic ice growth. Some variability in the radar ranges (and hence altitudes above the ground) of this general particle aspect ratio transition, however, was also observed.

The K_a -band cloud radar observations in a precipitating ice cloud at Oliktok Point indicated a range gradient of particle dominant shapes. The retrieved aspect ratios near the radar site were around 0.4, which is in good agreement with in-situ sampling results. Overall, it can be concluded that in spite of uncertainties in the aspect ratio retrievals, which could be as high as 0.2 or so, the DR-based approach of estimating particle shapes is rather robust and can provide quantitative information on dominant ice hydrometeor shapes.

Funding: This research was funded by the US Department of Energy's Atmospheric Systems Research (ASR) program (grant DE-SC0013306) and the National Science Foundation (grant AGS 1841260).

Conflicts of Interest: The author declares no conflicts of interest.

References

- 1. Vivekanandan, J.; Zrnic, D.S.; Ellis, S.M.; Oye, R.; Ryzhkov, A.V.; Straka, J. Cloud microphysics retrievals using S-band dual-polarization radar measurements. *Bull. Am. Meteorol. Soc.* **1999**, *80*, 381–388. [CrossRef]
- 2. Keenan, T. Hydrometeor classification with a C-band polarimetric radar. Aust. Meteorol. Mag. 2003, 52, 23–31.
- 3. Dolan, B.; Rutledge, S.A. A theory-based hydrometeor identification algorithm for X-band polarimetric radars. *J. Atmos. Ocean. Technol.* **2009**, *26*, 2071–2088. [CrossRef]

4. Hogan, R.L.; Tian, L.; Brown, P.R.A.; Westbrook, C.D.; Heymsfield, A.J.; Eastment, J.D. Radar scattering from ice aggregates using the horizontally aligned oblate spheroid approximation. *J. Appl. Meteorol. Climatol.* **2012**, *51*, 655–671. [CrossRef]

- 5. Jensen, A.A.; Harrington, J.Y.; Morrison, H.; Milbrandt, J.A. Predicting ice shape evolution in a bulk microphysics model. *J. Atmos. Sci.* **2017**, *74*, 2081–2104. [CrossRef]
- 6. Kokhanovsky, A.; Macke, A. The dependence of the radiative characteristics of optically thick media on the shape of particles. *J. Quant. Spectrosc. Radiat. Transf.* **1999**, *63*, 393–407. [CrossRef]
- 7. Bukovcic, P.; Ryzhkov, A.; Zrnic´, D.; Zhang, G. Polarimetric radar relations for quantification of snow based on disdrometer data. *J. Appl. Meteorol. Climatol.* **2018**, *57*, 103–120. [CrossRef]
- 8. Matrosov, S.Y. Theoretical study of radar polarization parameters obtained from cirrus clouds. *J. Atmos. Sci.* **1991**, *48*, 1062–1070. [CrossRef]
- 9. Matrosov, S.Y.; Reinking, R.F.; Kropfli, R.A.; Martner, B.E.; Bartram, B.W. On the use of radar depolarization ratios for estimating shapes of ice hydrometeors in winter clouds. *J. Appl. Meteorol.* **2001**, *40*, 479–490. [CrossRef]
- 10. Matrosov, S.Y.; Mace, G.G.; Marchand, R.; Shupe, M.D.; Hallar, A.G.; McCubbin, I.B. Observations of Ice crystal habits with a scanning polarimetric W-band radar at slant linear depolarization ratio mode. *J. Atmos. Ocean. Technol.* **2012**, *29*, 989–1008. [CrossRef]
- 11. Matrosov, S.Y.; Reinking, R.F.; Djalalova, I.V. Inferring fall altitudes of pristine dendritic crystals from polarimetric radar data. *J. Atmos. Sci.* **2005**, *62*, 241–250. [CrossRef]
- 12. Melnikov, V. Parameters of cloud ice particles retrieved from radar data. *J. Atmos. Ocean. Technol.* **2017**, 34, 717–728. [CrossRef]
- 13. Matrosov, S.Y.; Schmitt, C.G.; Maahn, M.; de Boer, G. Atmospheric ice particle shape estimates from polarimetric radar measurements and in situ observations. *J. Atmos. Ocean. Technol.* **2017**, *34*, 2569–2587. [CrossRef]
- 14. Jameson, A.R. Relations among linear and circular polarization parameters measured in canted hydrometeors. *J. Atmos. Ocean. Technol.* **1987**, *4*, 634–645. [CrossRef]
- 15. Melnikov, V.; Matrosov, S.Y. Estimations of aspect ratios of ice cloud particles with the WSR-88D radar. In Proceedings of the 36th Conference on Radar Meteorology, Breckenridge, CO, USA, 16–20 September 2013; American Meteorological Society: Washington, DC, USA, 2013; p. 245. Available online: https://ams.confex.com/ams/36Radar/webprogram/Paper228291.html (accessed on 21 October 2017).
- 16. Ryzhkov, A.; Matrosov, S.Y.; Melnikov, V.; Zrnic, D.; Zhang, P.; Cao, Q.; Knight, M.; Simmer, C.; Troemel, S. Estimation of depolarization ratio using weather radars with simultaneous transmission /reception. *J. Appl. Meteorol. Climatol.* **2017**, *56*, 1797–1816. [CrossRef]
- 17. Myagkov, A.; Seifert, P.; Wandinger, U.; Bühl, J.; Engelmann, R. Relationship between temperature and apparent shape of pristine ice crystals derived from polarimetric cloud radar observations during the ACCEPT campaign. *Atmos. Meas. Tech.* **2016**, *9*, 3739–3754. [CrossRef]
- 18. Matrosov, S.Y. Depolarization estimates from linear H and V measurements with radar radars operating in simultaneous transmission-simultaneous receiving mode. *J. Atmos. Ocean. Technol.* **2004**, *21*, 574–583. [CrossRef]
- 19. Moisseev, D.N.; Lautaportti, S.; Tyynela, J.; Lim, S. Dual-polarization radar signatures in snowstorms: Role of snowflake aggregation. *J. Geophys. Res.* **2015**, *120*, 12644–12655. [CrossRef]
- 20. Reinking, R.F.; Matrosov, S.Y.; Kropfli, R.A.; Bartram, B.W. Evaluation of a slant 45° slant quasi-liner radar polarization for distinguishing drizzle droplets, pristine ice crystals, and less regular ice particles. *J. Atmos. Ocean. Technol.* **2002**, *19*, 296–321. [CrossRef]
- 21. Marchand, R.; Mace, G.G.; Hallar, A.G.; McCubbin, I.B.; Matrosov, S.Y.; Shupe, M.D. Enhanced radar backscattering due to oriented ice particles at 95 GHz during Storm-VEx. *J. Atmos. Ocean. Technol.* **2013**, 30, 2336–2351. [CrossRef]
- 22. Von Lerber, A.; Moisseev, D.; Bliven, L.F.; Petersen, W.; Harri, A.M.; Chandrasekar, V. Microphysical properties of snow and their link to Ze-S relations during BAECC 2014. *J. Appl. Meteorol. Climatol.* **2017**, *56*, 1561–1582. [CrossRef]
- 23. Heymsfield, A.J.; Schmitt, C.; Bansemer, A. Ice cloud particle size distributions and pressure-dependent terminal velocities from in situ observations at temperatures from 0° to -86 °C. *J. Atmos. Sci.* **2013**, 70, 4123–4154. [CrossRef]

24. Matrosov, S.Y. A dual-wavelength radar method to measure snowfall rate. *J. Appl. Meteorol.* **1998**, 37, 1510–1521. [CrossRef]

- 25. Matrosov, S. Variability of microphysical parameters in high-altitude ice clouds: Results of the remote sensing method. *J. Appl. Meteorol.* **1997**, *36*, 633–648. [CrossRef]
- 26. Matrosov, S.Y.; Heymsfield, A.J. Empirical relations between size parameters of ice hydrometeor populations and radar reflectivity. *J. Appl. Meteorol. Climatol.* **2017**, *56*, 2479–2488. [CrossRef]
- 27. Matrosov, S.Y.; Campbell, C.; Kingsmill, D.; Sukovich, E. Assessing snowfall rates from X-band radar reflectivity measurements. *J. Atmos. Ocean. Technol.* **2009**, *26*, 2324–2339. [CrossRef]
- 28. Kennedy, P.C.; Rutledge, S.A. S-band dual-polarization radar observations of winter storms. *J. Appl. Meteorol. Climatol.* **2011**, *50*, 844–858. [CrossRef]
- 29. Bringi, V.N.; Chandrasekar, V. *Polarimetric Doppler Weather Radar*; Cambridge University Press: Cambridge, UK, 2001; 636p.
- 30. Matrosov, S.Y.; Shupe, M.D.; Djalalova, I.V. Snowfall retrievals using millimeter-wavelength cloud radars. *J. Appl. Meteorol. Climatol.* **2008**, *47*, 769–777. [CrossRef]
- 31. Atmospheric Radiation Measurement (ARM) User Facility. *Ka-Band Scanning ARM Cloud Radar* (*KASACRPPIVH*); 2016-10-20 to 2016-10-21, ARM Mobile Facility (OLI) Oliktok Point, Alaska, AMF3 (M1); Isom, B., Bharadwaj, N., Lindenmaier, I., Nelson, D., Hardin, J., Matthews, A., Eds.; ARM Data Center: Oak Ridge, TN, USA, 2018.
- 32. Matrosov, S.Y.; Maahn, M.; de Boer, G. Observational and modeling study of ice hydrometeor radar dual-wavelength ratios. *J. Appl. Meteorol. Climatol.* **2019**, *58*, 2005–2017. [CrossRef]
- 33. Sassen, K.; Matrosov, S.; Campbell, J. CloudSat spaceborne 94 GHz radar bright band in the melting layer: An attenuation driven upside-down lidar analog. *Geophys. Res. Lett.* **2007**, *34*, L16818. [CrossRef]



© 2020 by the author. Licensee MDPI, Basel, Switzerland. This article is an open access article distributed under the terms and conditions of the Creative Commons Attribution (CC BY) license (http://creativecommons.org/licenses/by/4.0/).